Contrib Mineral Petrol (2007) 153:85–103
DOI 10.1007/s00410-006-0136-x

ORIGINAL PAPER

The role of slab melting in the petrogenesis of high-Mg andesites: evidence from Simbo Volcano, Solomon Islands

S. König · S. Schuth · C. Münker · C. Qopoto

Received: 5 May 2006 / Accepted: 21 August 2006 / Published online: 12 October 2006

Abstract The petrogenesis of high-Mg andesites (HMA) in subduction zones involves shallow melting of refractory mantle sources or, alternatively, the interaction of ascending slab-derived melts with mantle peridotite. To unravel the petrogenesis of HMA, we report major, trace element and Sr–Nd–Hf–Pb isotope data for a newly found occurrence of HMA in the New Georgia group, Solomon Islands, SW-Pacific. Volcanism in the Solomon Islands was initiated by subduction of the Pacific plate beneath the Indian–Australian plate until a reversal of subduction polarity occurred ca. 10 Ma ago. Currently, the Indian–Australian plate is subducted northeastwards along the San Cristobál trench, forming the younger and still active southwestern Solomon island arc. However, a fossil slab of Pacific crust is still present beneath the arc. The edifice of the active volcano Simbo is located directly in the San Cristobál trench on top of the subducting Indian–Australian plate. Simbo Island lies on top of a strike-slip fault of the adjacent Woodlark spreading centre that is subducted beneath the Pacific plate. Geochemical and petrological compositions of volcanic rocks from Simbo are in marked contrast to those of volcanic rocks from islands north of the trench (mostly arc basalts). Simbo-type rocks are opx-bearing HMA, displaying 60–62 wt% SiO_2 but rather primitive Mg–Ni–Cr characteristics with 4–6 wt% MgO, up to 65 ppm Ni, up to 264 ppm Cr and Mg# from 67 to 75. The compositions of the Simbo andesites are explained by a binary mixture of silicic and basaltic melts. Relict olivine phenocrysts with $Fo_{88–90}$ and reaction-rims of opx also support a mixing model. The basaltic endmember is similar to back-arc basalts from the Woodlark Ridge. A slab melt affinity of the silicic mixing component is indicated by $Gd_{(N)}/Yb_{(N)}$ of up to 2.2 that is higher if compared to MORB and other arc basalts from the Solomon Islands. $^{87}Sr/^{86}Sr$, εNd and εHf values in the analysed rocks range from 0.7035 to 0.7040, +6.4 to +7.9 and +12 to +14.4, respectively. These values reveal the presence of the Indian–Australian mantle domain beneath Simbo (i.e. the Indian–Australian plate) and also beneath all other volcanic islands of the New Georgia group, which are located north of the San Cristobál trench. $^{206}Pb/^{204}Pb$, $^{207}Pb/^{204}Pb$ and $^{208}Pb/^{204}Pb$ values (18.43–18.52, 15.49–15.55 and 18.13–18.34, respectively) confirm the presence of slab melts from the subducted Pacific plate beneath southern Simbo where the highest $Gd_{(N)}/Yb_{(N)}$ ratios are reported. A spatial shift towards an Indian–Australian slab signature is observed when approaching the active San Cristobál trench on northern Simbo, reflecting the decreasing influence of slab melts from the old subducted Pacific plate.

Communicated by J. Hoefs.

S. König (✉) · S. Schuth · C. Münker
Institut für Mineralogie, Westfälische Wilhelms-Universität,
Corrensstrasse 24, 48149 Münster, Germany
e-mail: muchacho@uni-muenster.de

S. König · S. Schuth · C. Münker
Mineralogisch-Petrologisches Institut,
Friedrich-Wilhelms-Universität, Poppelsdorfer Schloss,
53115 Bonn, Germany

C. Qopoto
Department of Mines and Energy,
Ministry of Natural Resources, Lengakiki Road,
Honiara, Solomon Islands

Introduction

It is widely accepted that the source of present day arc-volcanism is mantle peridotite in the wedge above the subducting plate that was metasomatized due to dehydration and melting processes in subducted oceanic crust and sediment (e.g. Gill and Compston 1973; Ringwood 1974; Kay 1978, 1980; Perfit et al. 1980). Yet, most subduction-related magmas display variable proportions of components that originate from partial melting of the hydrated mantle wedge and components derived from both subducted sediments and subducted oceanic crust (e.g. Gill 1981; Nichols et al. 1994; Defant and Drummond 1990). The combined effects of these components on the petrogenesis of subduction-related magmas remain complex and are not yet fully understood. It was long assumed that present-day geotherms along subducting plates are too shallow to cause slab melting (e.g. Peacock et al. 1994), although more recent geophysical modelling (Kelemen et al. 2003) appears to require modification of this view. Moreover, recent experimental work (Kessel et al. 2005) suggests that there is an increasing miscibility between slab melts and slab fluids with depth. There is wide consensus that melting of subducted oceanic crust occurs in regions where young and hot oceanic crust is subducted or older subducting crust is torn (Yogodzinski 1995; Stern and Kilian 1996; Abratis and Wörner 2001). Adakites and high-Mg andesites (HMA) are believed to originate from variable interaction of parental tonalitic to dacitic melts with mantle peridotite during their ascent (e.g. Kay 1978, 1980; Martin 1986; Yogodzinski 1995).

Adakites are defined by SiO_2 contents of more than 56 wt%, more than 3 wt% Na_2O, between 3 and 6 wt% MgO and more than 600 ppm Sr (Defant and Drummond 1990). They also display extremely high Sr/Y ratios and low heavy-rare-earth element (HREE) concentrations (Y < 20 ppm, Yb < 1.9 ppm, Kay 1980; Defant and Drummond 1990). Known adakite occurrences include the Central Aleutians (Kay 1978, 1980), the Andean Austral zone (Stern and Kilian 1996) and Costa Rica (Abratis and Wörner 2001). The geochemical compositions of adakites appear to require hydrous, garnet-rich residues displaying initial trace element compositions that resemble mid-ocean-ridge basalts (MORBs, Defant and Drummond 1990). Adakites are referred to as modern analogues of Archaean TTG-suites, which reflect a higher geothermal gradient in the early Earth, thus generating large volumes of slab melts (Martin 1986; Defant and Drummond 1990; Martin and Moyen 2002). A steep geothermal gradient in the mantle wedge or deep melting (>150 km) is therefore regarded as major prerequisite for the partial melting of subducted oceanic crust (e.g. Peacock et al. 1994; Stern and Kilian 1996; Kessel et al. 2005).

The HMA are broadly characterized by high Mg#, elevated MgO, Cr- and Ni-concentrations at SiO_2 contents between 53 and 63 wt% (e.g. Crawford et al. 1989). This broad definition, however, includes boninites that have no slab melt component but are restricted to volcanic rocks with MgO contents of more than 8 wt%, SiO_2 contents above 52 wt% and less than 0.5 wt% TiO_2 (Le Bas 2000). The occurrences of boninites are associated with modern subduction zone environments such as the Bonin Islands (e.g. Petersen 1891), Cape Vogel, Papua New Guinea (e.g. Dallwitz et al. 1966), the Mariana Trench (e.g. Dietrich et al. 1978), New Caledonia (e.g. Meffre et al. 1996) and the Setouchi volcanic belt (Tatsumi 1982). Key condition for boninite generation is the addition of large amounts of hydrous fluids into refractory peridotite in order to lower the solidus temperatures, thus triggering partial melting at depths of less than 50 km (Crawford et al. 1989).

In addition to boninites, melts with adakitic affinities that have assimilated mantle peridotite or basaltic melts constitute a second group of HMA. In this case, the bulk geochemistry of HMA results from reactions between adakitic melts and peridotites in the mantle wedge (Yogodzinski 1995), displaying trace element compositions that are transitional between adakites and typical island arc andesites (e.g. Sr/Y ratios less than 100 but still unusually high). Modern occurrences of this HMA group include the New Hebrides (e.g. Monzier et al. 1993), the Aleutians (e.g. Yogodzinski 1995), Kamchatka (e.g. Kepezhinskas et al. 1995; Yogodzinski et al. 2001), the Cascades (e.g. Grove et al. 2002) and the Andean Austral volcanic zone in South America (e.g. Stern and Kilian 1996). HMA that only contain small amounts of slab melts can often only be recognized by their trace element characteristics.

In order to assess the role of slab melts during the petrogenesis of HMA, we examined HMA from the New Georgia archipelago in the Solomon Islands. Our study focuses on the geochemistry, tectonic setting and petrogenesis of the New Georgia HMA as well as their genetic relationship to associated typical arc basalts and andesites. The New Georgia HMA that mainly occur on the island of Simbo are the most MgO-rich andesites at a given SiO_2 concentration amongst all other andesites found in the Solomon Islands (see Schuth et al. 2004). Companion studies by Schuth et al.

(2004) and Rohrbach et al. (2005) already assessed the geochemical and petrological characteristics of basalts and picrites occurring in the New Georgia group. Here, we present new major, trace element and Hf–Sr–Nd–Pb isotope data for New Georgia HMA. Based on the data, a petrogenetic model is developed and the significance of slab melting processes for the general petrogenetic understanding of HMA is evaluated.

Geological setting

The Solomon island arc is a ca. 800 km long double chain of volcanic islands that is located on the southwestern border of the Pacific plate (Fig. 1). The

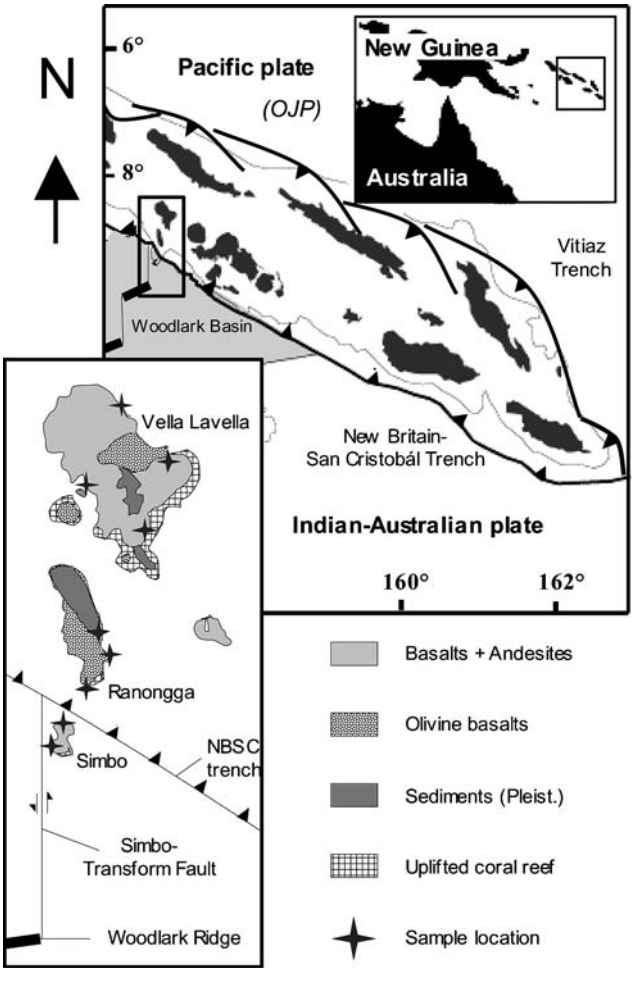

Fig. 1 Simplified geological and tectonic map of the western part of the New Georgia group (after Abraham et al. 1987; Mann et al. 1998). The Ontong Java Plateau (OJP) makes up most of the Pacific plate in this area. Note that Simbo Island is located south of the NBSC trench on the subducting edge of the Indian–Australian plate

formation of the northeastern island chain of the Solomons was triggered by subduction of the Pacific plate beneath the Indian–Australian plate along the Vitiaz trench during Eocene time (Petterson et al. 1999). Arc-volcanism ceased in the upper Oligocene after the collision of the arc with the Ontong Java Plateau (OJP) that was formed on the Pacific plate by plume magmatism at 120–90 Ma (e.g. Tejada et al. 2004). However, subduction processes along the Vitiaz trench are believed to be still active, as minor seismic activity is still recorded (e.g. Mann 1997; Cowley et al. 2004; Mann and Taira 2004). Due to the thickness of the OJP (more than 30 km, e.g. Hussong et al. 1979; Miura et al. 2003) and its rigidity, the collision with the Indian–Australian plate led to a reversal in subduction polarity. Arc-volcanism above the now subducting Indian–Australian plate started ca. 6 Ma ago (Petterson et al. 1999), forming the southwestern volcanic chain of the Solomon Islands that is still active.

Presently, the Pacific plate moves northwestwards with 10 cm/a and is intercepted at high angle by the Indian–Australian plate that moves with 7 cm/a to the northeast (Petterson et al. 1999). The islands of the New Georgia group form part of the active southwestern Solomon island arc and lie on the Pacific plate with a distance of less than 50 km to the New Britain–San Cristobál (NBSC) trench (Fig. 1). As a particular feature of the Solomon arc, the Woodlark Ridge (WR) spreading centre of the Indian–Australian plate is subducted beneath the New Georgia group. Spreading along the WR began at ca. 4 Ma (e.g., Mann et al. 1998). The subduction of young and hot oceanic crust explains the lower seismic activity reported for the New Georgia group compared to other sections of the arc (Mann 1997). Via adiabatic decompression, the still active spreading centre supplies extra heat to the mantle wedge beneath the active Solomon arc, causing an elevated temperature gradient. As a consequence, the active Solomon arc is located less than 50 km behind the NBSC trench (Marshak and Karig 1977).

Although being part of the western New Georgia group, the island of Simbo has a unique tectonic setting. Geophysical data indicate a position of Simbo in vicinity of the NBSC trench. In contrast to all other islands of the Solomon arc, Simbo Island is located on the edge of the Indian–Australian plate, immediately on top of a strike-slip fault that is associated with the adjacent Woodlark spreading centre (Yoneshima et al. 2005; Fig. 1). Less than 20 km to the north of Simbo, the island of Ranongga is located on the Pacific plate, to the north of the NBSC trench. The island of Vella Lavella is located another 40 km further north of Ranongga. To elucidate the plate tectonic control on

the composition of the volcanic rocks, we examined samples from all three islands.

Basaltic and andesitic volcanic centres form the largest parts of Vella Lavella. In contrast, the adjacent island of Ranongga that is located closer to the trench than Vella Lavella is part of the forearc region. Northern Ranongga mainly consists of clastic sediments, whereas basaltic rocks with minor outcrops of andesites dominate southern Ranongga. In contrast to the other two islands, Simbo consists only of andesitic cones (Abraham et al. 1987). Exact ages of any of the three islands are unknown, but can be confined to less than 4 Ma based on the morphology and tectonic position. Volcanism on some of the islands is still active. Clear evidence for recent historic activity is restricted to Simbo, where hot springs, solfatares and recent sulphur deposits are abundant. Minor post-volcanic activity (hot springs) also occurs on Vella Lavella. Rapid uplift in the region is indicated by Holocene coral reefs that are now above sea level. Uplift rates of up to 7.5 cm/a are recorded in the forearc (Mann et al. 1998).

Sampling and analytical methods

The samples examined in this study were collected from the islands of Simbo, Ranongga and Vella Lavella, thus sampling an across-arc section. Due to intense weathering, most samples were taken from creek boulders with known source catchments or shoreline outcrops. Only fresh cores of rocks, displaying visibly unaltered phenocrysts, were considered for analysis. A set of 24 samples was analysed by X-ray fluorescence (XRF) analysis. From the group of 24 samples, 15 were chosen for incompatible trace element analyses by quadrupole inductively coupled-plasma mass spectrometry (quadrupole ICP-MS) and isotope measurements. Thermal ionization mass spectrometry (TIMS) was used for Sr–Nd–Pb isotope analyses whereas Hf isotope compositions were analysed using multiple collector-inductively coupled plasma-mass spectrometry (MC-ICP-MS). Phenocrysts of two samples were analysed by electron microprobe. Sixteen representative samples were analysed for their Sr–Nd–Hf–Pb isotope compositions.

The samples were crushed in a steel jaw-crusher and ground in an agate mill. Major elements were determined using a Philips PW-1480 XRF spectrometer at the Universität Bonn. Rare earth elements and Sc, Rb, Sr, Y, Zr, Nb, Sb, Cs, Ba, Hf, Ta, Pb, Th, U were analysed using an Agilent 7500cs quadrupole ICP-MS at the Universität Kiel. For quadrupole ICP-MS measurements, ca. 100 mg of the samples were dissolved in concentrated HF/HNO_3 (5:1) at 200°C for 24 h in Savillex® vials placed inside Parr® Teflon bombs. After three repeated dry down steps with concentrated HNO_3, the residue was completely dissolved in 6 ml HNO_3/H_2O (1:2) and diluted in 50 ml H_2O, yielding a final concentration of ca. 2% HNO_3. Prior to analysis, an internal In–Re standard was added. For collisional thermalization, a gas flow of 1.1 ml He per minute was applied in the reaction cell, leading to an improved internal precision of <1% RSD over 10 h for most elements. A comparison of results for the BIR standard with recommended values of Govindaraju (1994) is given in Table 1. The FeO content of each sample was determined by visual titration using 120 mg of the sample and a 0.02 N solution of $KMnO_4$ (Heinrichs and Herrmann 1990). The external reproducibility was better than 5%.

Sr–Nd–Hf results were all obtained from one split of ca. 100 mg sample powder. Hafnium was separated using the one-column Eichrom Ln Spec procedure of Münker et al. (2001). From the remaining matrix, Sr and Nd were separated using conventional ion exchange methods.

Table 1 Measured trace element concentrations for the BIR-1 standard ($n = 1$) compared to recommended values from Govindaraju (1994) and Weyer et al. (2003) (Nb, Ta, Zr, Hf)

Element	BIR-1 measured	BIR standard (Lit.)
Sc	50	44
Rb	0.21	0.25
Sr	94	108
Y	14	16
Zr	13.5	14
Nb	0.56	0.55
Cs	0.003	0.005
Ba	6.8	7.0
La	0.63	0.62
Ce	1.95	1.95
Pr	0.38	0.38
Nd	2.4	2.5
Sm	1.1	1.1
Eu	0.54	0.54
Gd	1.76	1.85
Tb	0.36	0.36
Dy	2.6	2.5
Ho	0.57	0.57
Er	1.6	1.7
Tm	0.25	0.26
Yb	1.69	1.65
Lu	0.26	0.26
Hf	0.56	0.58
Pb	0.54	3.0
Th	0.05	0.03
U	0.01	0.01

Note that the BIR-1 standard used in this study is an aliquot of the original uncrushed USGS standard that was separately ground in an agate mill by C. Münker, thus explaining the large difference in Pb concentrations

The Sr–Nd isotope compositions were measured using the Thermo-Finnigan Triton TIMS at Münster operated in static mode. $^{87}Sr/^{86}Sr$ and $^{143}Nd/^{144}Nd$ were normalized to $^{84}Sr/^{86}Sr = 0.1194$ and $^{146}Nd/^{144}Nd = 0.7219$, respectively. Repeated analyses of the standards NBS 987 (for Sr) and La Jolla (for Nd) during the course of the measurements gave mean values of 0.710257 ($n = 4$) and 0.511846 ($n = 4$), respectively. Long-term external reproducibilities for $^{87}Sr/^{86}Sr$ and $^{143}Nd/^{144}Nd$ are ± 30 ppm. Hafnium isotope compositions were determined using the Micromass IsoProbe MC-ICP-MS at Münster. An average value of 0.282130 with a long-term reproducibility of ± 50 ppm was measured for the Münster AMES Hf-standard, which is isotopically indistinguishable from the JMC-475 Hf-standard. All results are given relative to a $^{176}Hf/^{177}Hf$ value of 0.282160 for the AMES/JMC-475 standards. εHf and εNd values were calculated using CHUR values of $^{176}Hf/^{177}Hf = 0.282772$ from Blichert-Toft and Albaréde (1997) and $^{143}Nd/^{144}Nd = 0.512683$ from Jacobsen and Wasserburg (1980) for normalization.

For Pb isotope analyses, ca. 3 mm sized whole-rock chips were put in an ultrasonic bath for 15 min, repeatedly washed with H_2O and then dried at 80°C for 2 h. Subsequently, 150 mg were leached in hot 6 N HCl for 1 h in Savillex® vials. The HCl was removed and the vials containing the chips were washed with H_2O. This step was repeated using 3 N HCl. The grains were then completely dissolved in HF/HNO_3 at 120°C for 12 h in Savillex® vials. Pb was separated using anion exchange techniques.

The Pb isotope compositions were measured using the VG Sector 54 TIMS at Münster operated in static mode. In order to correct for mass-fractionation, an average mass bias was determined by repeated NBS 982 measurements, and the values from Todt et al. (1996) were used for mass bias correction. Repeated analyses of the NBS 982 standard yielded a typical mass fractionation of 1.4‰ per a.m.u. and an external reproducibility of 0.44‰ per a.m.u.. The NBS 982 standard and three samples were additionally analysed for their Pb isotope compositions using the Thermo-Finnigan Triton. The difference between NBS 982 measured, using both Triton and VG Sector 54 TIMS, ($^{206}Pb/^{204}Pb$ ± 0.014, $^{207}Pb/^{204}Pb$ ± 0.031 and $^{208}Pb/^{204}Pb$ ± 0.007) was within the external reproducibility. Results of the Sr–Nd–Hf–Pb isotope analyses are given in Table 2.

Results

Petrography

Petrographically, two distinct groups of volcanic rocks can be distinguished. Orthopyroxene-bearing andesites

Table 2 Sr–Nd–Hf–Pb isotope data from MC-ICP-MS and TIMS analyses

Sample	$^{176}Hf/^{177}Hf \pm 2\sigma$	εHf	$^{87}Sr/^{86}Sr \pm 2\sigma$	$^{143}Nd/^{144}Nd \pm 2\sigma$	εNd	$^{206}Pb/^{204}Pb$	$^{207}Pb/^{204}Pb$	$^{208}Pb/^{204}Pb$
VL 102	0.283154 ± 10	13.5	0.703471 ± 16	0.513011 ± 16	+7.3	18.43	15.54	38.16
VL 103	0.283170 ± 9	14.1	0.703821 ± 14	0.513021 ± 16	+7.5	18.43	15.50	38.14
	0.283169 ± 10	14.0	0.703817 ± 12					
VL 110	0.283154 ± 10	13.5	0.703530 ± 16	0.513019 ± 16	+7.4	18.47	15.51	38.24
VL 111	0.283145 ± 10	13.2	0.703757 ± 14	0.513015 ± 16	+7.4			
RG 113	0.283161 ± 10	13.8	0.703517 ± 16	0.513042 ± 12	+7.9	18.52	15.51	38.25
RG 117	0.283147 ± 7	13.3	0.704041 ± 18	0.512967 ± 12	+6.4	18.54	15.51	38.28
	0.283141 ± 7	13.1						
RG 118	0.283168 ± 8	14.0	0.703652 ± 16	0.513012 ± 14	+7.3	18.55	15.56	38.42
RG 119	0.283179 ± 7	14.4	0.703560 ± 14	0.512996 ± 14	+7.0	18.51	15.50	38.22
SB 121	0.283112 ± 7	12.0	0.703517 ± 12	0.513035 ± 12	+7.7	18.52	15.50	38.15
SB 123	0.283110 ± 7	12.0	0.703564 ± 14	0.513023 ± 14	+7.5	18.54	15.53	38.25
						18.54[a]	15.54[a]	38.29[a]
SB 125	0.283137 ± 9	12.9	0.703549 ± 14	0.512992 ± 18	+6.9	18.43	15.49	38.13
	0.283128 ± 9	12.6						
SB 126	0.283132 ± 9	12.7	0.703530 ± 14	0.512981 ± 14	+6.7	18.43	15.53	18.22
SB 128	0.283125 ± 9	12.5	0.703565 ± 14	0.513014 ± 16	+7.3	18.49	15.55	38.34
SB 129	0.283133 ± 7	12.8	0.703495 ± 12	0.512973 ± 14	+6.5	18.47	15.53	38.29
RG 131	0.283172 ± 9	14.1	0.703666 ± 14	0.512996 ± 18	+7.0	18.51[a]	15.54[a]	38.36[a]
						18.52[a]	15.57[a]	38.45[a]
SB 132	0.283134 ± 7	12.8	0.703522 ± 14	0.512996 ± 14	+7.0	18.47[a]	15.52[a]	38.22[a]
SB 133b	0.283122 ± 7	12.4	0.703600 ± 14	0.512977 ± 16	+6.6	18.43	15.49	38.15

εNd and εHf were calculated with CHUR values from Jacobsen and Wasserburg (1980) and Blichert-Toft and Albaréde (1997), respectively

[a] Some Pb data were obtained using a different TIMS (see text for details)

are confined to the Simbo Island whereas amphibole and clinopyroxene-bearing basalts and basaltic andesites make up the islands of Vella Lavella and Ranongga. The Ranongga and Vella Lavella suite is porphyric, containing 15–30 vol.% plagioclase phenocrysts of up to 1 mm in size and 3–7 vol.% clinopyroxene (cpx) with diameters ranging from 1 to 2 mm. Additionally, two samples from Vella Lavella (VL 104, VL 110) contain amphibole megacrysts of up to 7 mm in diameter. Olivine is rare and crystal sizes do not exceed 2.5 mm. An exception is sample VL 103 with up to 10 vol.% olivine. Olivines in sample RG 117 are exceptionally altered. The Simbo andesites display zoning in their plagioclase phenocrysts that have diameters of up to 12 mm and are embedded in a matrix that is occasionally glassy. Orthopyroxene sizes typically range from 1 to 7 mm. Vesicles are rare in all samples. A characteristic feature of the Simbo andesites is the xenomorphic olivines that are surrounded by orthopyroxene rims (Fig. 2a). Electron microprobe analyses yielded Fo# values of 88–90 for the olivines (Table 3). CaO contents of the olivines range from 0.13 to 0.20 wt% and are intermediate between mantle olivines and basaltic/picritic solidus olivines in other Solomon Island basalts (cf. Rohrbach et al. 2005). The presence and textural relationships of these olivines indicate mixing between an olivine-rich component and a silicic melt where subsequent equilibration reactions produced the opx rims. This is also supported by Ni concentrations in olivines and orthopyroxenes from Simbo-type andesites (Fig. 2b). The Ni contents are unusually high for orthopyroxenes. Due to the disequilibrium between the olivine and surrounding SiO_2-rich melt which produced opx, Ni is forced into the opx structure in spite of the low $D_{opx/L}$ for Ni.

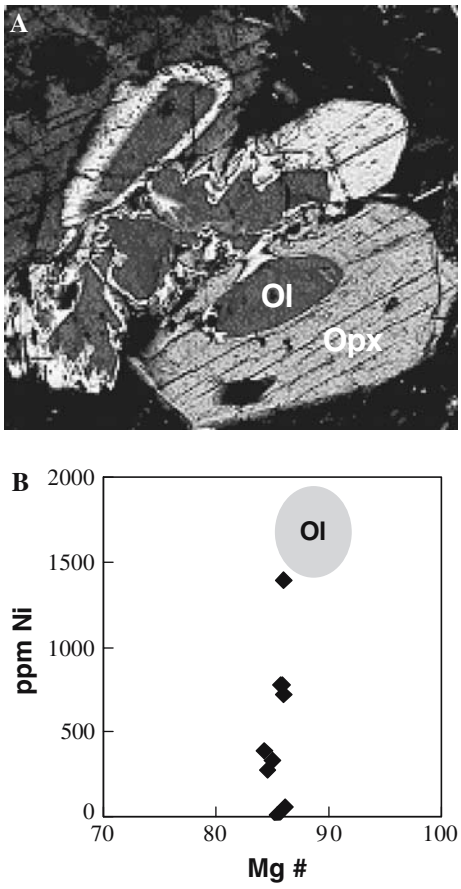

Fig. 2 **a** Cores of xenocrystic olivine with surrounding rims of orthopyroxene, indicating equilibration reactions during binary mixing of SiO_2-rich and mafic endmembers. Width of field is 30 μm. Results of electron microprobe analyses of the area shown are given in **b** and Table 3 (sample SB 121). **b** Ni concentrations in olivine (*grey field*) and orthopyroxene (*filled diamonds*) from Simbo-type andesites. Due to the disequilibrium between the olivine and surrounding SiO_2-rich melt which produced opx, Ni is forced into the opx structure in spite of the low $D_{opx/L}$ for Ni

Major and trace element composition

The distinction between the two petrographic groups is confirmed by major and trace element compositions (Table 4). On the basis of the total alkali versus silica (TAS) diagram (after Le Bas 2000; Fig. 3), the Ranongga and Vella Lavella basalts and basaltic andesites display SiO_2 contents of 49–57 wt% and differ from the Simbo andesites with SiO_2 contents of 60–62 wt% and a narrow range of total alkaline contents (3.2–4.2 wt%). A general decrease of MgO, FeO and CaO concentrations with increasing SiO_2 and Al_2O_3 contents indicates a typical calc-alkaline fractional crystallization trend for the Ranongga and Vella Lavella suite (Fig. 4). For the Simbo andesites, however, the MgO contents are distinctively higher, ranging from 4 to 6 wt% at SiO_2 concentrations of ca. 60 wt%, which is typical for HMA. The Mg# values in the Simbo andesites range from 67 to 75, overlapping with values from primitive basaltic melts. In accord with the high MgO contents, the compatible trace elements Ni and Cr show relatively high concentrations in the Simbo andesites of 15–50 ppm for Ni and 50–250 ppm for Cr, compared to 5–55 ppm Ni and 20–200 ppm Cr in the Ranongga and Vella Lavella suite. In comparison to the Ranongga and Vella Lavella suite, the Simbo andesites also have the lowest CaO concentrations of 6.5–8.5 wt% and the lowest Fe_{tot} content with 6–7 wt%. Concentrations of the incompatible trace elements Zr, Th, Ba, Rb are lower in the Simbo andesites than in the suite from Ranongga and Vella Lavella. A characteristic decrease in Zr concentrations with increasing SiO_2 contents can be observed in the Simbo andesites.

Table 3 Electron microprobe data obtained for samples SB 121, SB 125

Sample	Phase	Mg#	SiO_2 (wt%)	MgO (wt%)	CaO (wt%)	Al_2O_3 (wt%)	FeO (wt%)	Ni (ppm)	Cr (ppm)
SB 121	ol	72.5	40.5	49.3	0.146	0.015	10.5	1,775	102
	opx	65.9	56.8	31.5	1.71	0.652	9.15	55.0	1,980
	ol	71.1	40.6	49.4	0.134	0.019	11.3	1,775	204
	opx	64.6	55.8	31.0	1.72	1.30	9.53	7.86	2,993
	ol	69.9	40.7	48.0	0.132	<0.01	11.6	1,500	801
	opx	63.8	55.6	30.6	1.97	1.11	9.74	330	2,058
	opx core	62.4	56.1	31.4	1.89	0.733	10.6	385	1,878
	cpx	65.4	53.1	18.4	20.7	1.38	5.47	502	4,015
	opx	63.0	56.2	30.9	1.78	0.621	10.2	777	345
	opx	65.7	55.7	31.6	1.94	1.08	9.25	275	2,514
	ol core	71.5	40.4	48.9	0.201	0.043	10.9	1,830	212
	opx core	65.2	56.1	31.6	1.65	0.527	9.50	722	636
	opx rim	65.6	55.9	31.2	1.85	0.751	9.19	777	1,139
	opx rim	61.2	56.2	30.8	1.76	0.590	10.9	1,390	573
SB 125	opx	58.0	55.3	29.3	1.96	1.39	11.9	440	1,092
	opx	60.2	55.5	30.1	1.71	1.50	11.2	385	911
	opx	84.2	53.6	22.4	1.41	0.541	23.6	275	275

Incompatible trace element systematics indicate variable enrichments in light rare earth elements (LREE) relative to HREE for all groups (Fig. 5). A striking feature, however, is that the HREE concentrations in the Simbo andesites (5 × chondritic) are depleted by a factor of up to 3 relative to those in the other samples. The HREE depletions in the Simbo andesites result in $La_{(N)}/Yb_{(N)}$ ratios (5.2–10.4) that are higher than in the basalts and basaltic andesites ($La_{(N)}/Yb_{(N)}$ from 1.4 to 3.2; Table 4). An exception is the basaltic sample RG 117 from southern Ranongga ($La_{(N)}/Yb_{(N)}$ of 7.8) that rather matches the values found in the Simbo andesites. This observation could be explained by the short geographic distance between southern Ranongga and the Simbo Island and, hence, by a similar petrogenesis. The sample is therefore discussed with the group of Simbo andesites. The Simbo andesites display higher SiO_2 contents than all the other samples, and the observed differences in REE contents suggest that the magmatic sources of the two groups are strikingly different.

Both groups show selective enrichments of the fluid-mobile elements Rb, Ba, K, Pb and Sr and depletions in the HFSE relative to N-MORB which is a characteristic feature of subduction-related volcanic rocks (Fig. 6). The Simbo andesites also display strong enrichments in Th and U. Europium anomalies are also restricted to this group and show Eu/Eu* values between 0.7 and 1. The compositional affinities of the Simbo andesites to subduction zone rocks are surprising, given that these rocks erupted above a transform fault that is part of an active spreading centre.

Sr–Nd–Hf–Pb isotope compositions

Sixteen representative samples from Simbo, Ranongga and Vella Lavella were analysed for their Sr–Nd–Hf–Pb isotope compositions. $^{87}Sr/^{86}Sr$ values range from 0.7034 to 0.7040; most samples have values below 0.7036. Sample RG 117 from Ranongga displays the highest $^{87}Sr/^{86}Sr$ value of 0.7040 that is possibly related to weathering as suggested by the presence of altered olivines observed in thin sections. Epsilon Nd values range from +6.4 to +8.3, with most samples scattering around +7.0. However, all samples from Vella Lavella display εNd values above +7.3. εHf values vary between +12.0 and +14.4 with systematically lower εHf values for Simbo-type rocks compared to rocks from Ranongga and Vella Lavella. Values in the Simbo andesites range from +12.0 to +12.9 and values in the Ranongga and Vella Lavella suite range from +13.1 and +14.4. The Sr–Nd–Hf data obtained in this study overlap with those obtained by Schuth et al. (2004) for all other islands of the New Georgia group (Fig. 7a) and plot into or close to the Indian MORB field in Hf–Nd isotope space (Fig. 7b). Lead isotope compositions range from $^{206}Pb/^{204}Pb$ = 18.43 to 18.55, $^{207}Pb/^{204}Pb$ = 15.49 to 15.56 and $^{208}Pb/^{204}Pb$ = 38.13 to 38.42, respectively. These values plot into the Pacific MORB field (Fig. 11; Kempton et al. 2002), clearly revealing a significant influence of components derived from the Pacific plate (subducted until ca. 12 Ma B.P.) on the examined volcanic rocks. The influence of pelagic marine sediments appears to be negligible (Fig. 11).

Table 4 XRF and ICP-MS data for 24 samples

Sample	VL 102	VL 103	VL 104	VL 110	VL 111	RG 113	RG 115	RG 117	RG 118	RG 119	SB 120	SB 121	SB 122	SB 123	SB 124	SB 125	SB 126	SB 127	SB 128	SB 129	SB 131	SB 132	SB 133[a]	SB 133[b]
SiO_2	55.0	50.1	54.3	53.1	55.5	54.3	51.0	48.2	54.2	56.5	61.9	60.9	60.8	60.9	61.3	60.8	61.7	61.2	61.7	60.0	55.0	59.0	61.9	61.2
TiO_2	0.740	0.806	0.658	0.741	0.684	0.581	0.667	0.684	0.587	0.558	0.432	0.454	0.455	0.426	0.454	0.469	0.486	0.467	0.486	0.516	0.661	0.556	0.465	0.466
Al_2O_3	17.3	14.1	18.2	18.4	17.8	15.7	15.6	13.4	15.8	16.6	14.1	13.6	14.0	13.7	14.4	14.6	15.2	14.8	14.7	14.1	17.2	13.8	15.0	15.0
FeO	4.38	5.22	3.23	2.91	3.21	1.36	6.33	5.54	5.40	4.32	3.73	4.10	3.41	3.40	3.20	2.86	2.53	3.30	3.32	4.40	4.35	4.44	3.72	3.86
Fe_2O_3	3.50	4.79	5.69	5.66	4.49	6.42	4.07	5.43	3.49	3.16	2.46	2.24	2.87	2.94	3.10	3.21	3.47	2.70	2.80	2.57	3.52	2.85	2.34	2.43
MnO	0.153	0.181	0.141	0.162	0.174	0.143	0.182	0.197	0.162	0.132	0.11	0.111	0.111	0.102	0.111	0.102	0.101	0.102	0.101	0.122	0.15	0.121	0.101	0.112
MgO	3.67	10.6	3.73	3.82	3.05	6.73	6.87	8.30	5.97	5.15	5.40	6.02	5.62	5.57	4.87	4.55	3.99	4.47	4.44	5.40	4.70	5.78	4.19	4.33
CaO	8.03	9.84	9.01	9.36	8.07	10.1	11.4	9.88	10.4	8.81	7.74	7.87	7.61	7.82	7.91	7.75	7.36	7.61	7.02	8.33	9.27	8.60	7.44	7.58
Na_2O	3.37	2.23	2.89	2.94	3.03	1.67	1.71	2.30	1.72	1.99	2.16	1.98	2.16	2.01	2.22	2.31	2.43	2.29	2.36	1.87	2.43	2.05	2.33	2.33
K_2O	1.66	1.06	1.22	1.36	1.76	1.04	0.93	2.39	0.88	1.18	1.47	1.6	1.55	1.50	1.42	1.30	1.36	1.37	1.58	1.45	0.99	1.25	1.39	1.35
P_2O_5	0.30	0.210	0.135	0.20	0.224	0.150	0.159	0.340	0.140	0.140	0.108	0.160	0.154	0.130	0.109	0.110	0.110	0.112	0.120	0.120	0.130	0.170	0.107	0.103
LOI	0.140	0.001	0.450	0.63	0.98	1.00	0.18	2.69	0.27	0.65	0.001	0.390	0.610	0.470	0.490	0.080	0.060	0.440	0.520	0.001	0.40	0.010	0.10	0.020
Total	98.3	99.1	99.6	99.2	99.0	99.1	99.1	99.1	99.0	99.1	99.5	99.5	99.6	99.0	99.7	98.2	98.9	98.9	99.3	99.8	100	99.0	99.1	98.7
Mg#	60.3	78.5	67.7	70.5	63.5	89.7	66.3	73.6	66.6	68.4	72.3	72.5	74.8	73.7	73.3	74.0	74.2	71.1	70.9	68.9	65.6	70.3	67.1	67.3
Sc	27.0	37.7	–	24.8	–	41.3	–	37.4	45.3	33.3	–	33.8	–	34.1	–	33.3	–	–	31.5	38.1	32.1	40.1	–	33.1
V	262	294	–	263	–	309	–	331	331	280	–	238	–	236	–	226	–	–	227	275	283	272	–	238
Cr	39.0	675	–	14.5	–	225	–	291	158	158	–	264	–	210	–	82.5	–	–	75.2	149	52.3	192	–	53.0
Ni	17.9	283	–	13.9	–	67.8	–	95.1	45.4	55.0	–	64.2	–	48.1	–	30.6	–	–	31.3	34.0	33.5	37.7	–	25.4
Zn	84.5	81.0	–	80.1	–	65.7	–	88.1	72.8	64.3	–	57.8	–	55.3	–	54.5	–	–	58.4	60.7	75	63.5	–	62.3
Rb	32.0	18.9	–	24.0	–	19.5	–	49.9	15.3	19.2	–	33.2	–	30.5	–	24.0	–	–	25.0	26.1	16.3	25.0	–	24.5
Sr	702	480	–	704	–	331	–	875	326	415	–	635	–	622	–	411	–	–	607	553	379	524	–	433
Y	18.9	20.5	–	20.2	–	15.4	–	16.7	16.5	16.6	–	14.1	–	14	–	13.7	–	–	13.0	13.7	18.5	15.8	–	14.0
Zr	78.7	57.3	–	67.1	–	30.1	–	57.5	29.3	38.3	–	126.6	–	115	–	86.3	–	–	93.7	90.4	45.4	112	–	86.3
Nb	2.15	1.16	–	1.39	–	0.590	–	2.01	0.71	0.98	–	3.17	–	2.09	–	2.08	–	–	2.14	2.40	0.770	2.50	–	1.96
Sb	0.0722	0.0374	–	0.0645	–	0.0235	–	0.0928	0.0267	0.0317	–	0.0638	–	0.0687	–	0.0783	–	–	0.0863	0.0649	0.0638	0.0649	–	0.0853
Cs	0.203	0.256	–	0.456	–	0.233	–	0.439	0.179	0.246	–	0.397	–	0.378	–	0.323	–	–	0.226	0.305	0.264	0.250	–	0.347
Ba	265	122	–	204	–	80.2	–	222	77.9	105	–	233	–	231	–	180	–	–	296	183	130	194	–	185
La	8.40	6.36	–	9.61	–	3.51	–	18.96	4.34	5.97	–	21.76	–	19.4	–	10.9	–	–	13.5	15.1	5.29	17.1	–	11.6
Ce	18.7	14.7	–	20.1	–	7.80	–	39.2	9.41	12.6	–	47.6	–	43.2	–	23.8	–	–	28.9	32.1	11.5	36.8	–	25.2
Pr	2.80	2.18	–	2.85	–	1.15	–	4.87	1.37	1.71	–	6.23	–	5.59	–	3.12	–	–	3.77	4.06	1.67	4.91	–	3.29
Nd	11.8	10.2	–	12.6	–	5.62	–	19.5	6.60	7.74	–	25.0	–	22.8	–	12.3	–	–	14.6	16.1	7.60	20.1	–	12.8
Sm	2.89	2.76	–	3.08	–	1.72	–	3.93	1.92	2.07	–	4.61	–	4.32	–	2.50	–	–	2.82	3.02	2.18	3.99	–	2.56
Eu	0.794	0.957	–	1.06	–	0.633	–	1.17	0.683	0.709	–	1.19	–	1.10	–	0.560	–	–	0.610	0.800	0.690	1.07	–	0.560
Gd	2.96	3.21	–	3.37	–	2.17	–	3.81	2.35	2.42	–	3.86	–	3.58	–	2.31	–	–	2.4	2.77	2.55	3.58	–	2.36
Tb	0.476	0.527	–	0.536	–	0.377	–	0.535	0.405	0.407	–	0.483	–	0.46	–	0.36	–	–	0.36	0.39	0.44	0.49	–	0.360
Dy	2.94	3.38	–	3.39	–	2.54	–	3.07	2.71	2.68	–	2.51	–	2.45	–	2.14	–	–	2.06	2.28	2.86	2.74	–	2.13
Ho	0.612	0.70	–	0.699	–	0.539	–	0.597	0.582	0.57	–	0.483	–	0.48	–	0.45	–	–	0.420	0.460	0.600	0.540	–	0.450
Er	1.76	1.99	–	2.02	–	1.56	–	1.66	1.69	1.65	–	1.37	–	1.37	–	1.32	–	–	1.23	1.36	1.76	1.54	–	1.31
Tm	0.263	0.300	–	0.306	–	0.241	–	0.241	0.257	0.257	–	0.203	–	0.203	–	0.189	–	–	0.189	0.206	0.275	0.232	–	0.208
Yb	1.78	2.04	–	2.11	–	1.68	–	1.63	1.78	1.78	–	1.41	–	1.41	–	1.43	–	–	1.33	1.44	1.86	1.59	–	1.44
Lu	0.270	0.310	–	0.330	–	0.260	–	0.240	0.270	0.280	–	0.210	–	0.219	–	0.219	–	–	0.201	0.230	0.285	0.245	–	0.217
Hf	1.9	1.65	–	1.82	–	1.00	–	1.65	1.00	1.23	–	3.00	–	2.79	–	2.21	–	–	2.41	2.52	1.26	2.72	–	2.17
Pb	2.75	2.30	–	2.94	–	1.92	–	5.86	1.89	2.38	–	5.01	–	4.88	–	3.38	–	–	4.31	3.70	2.07	3.57	–	3.48

Table 4 continued

Sample	VL 102	VL 103	VL 104	VL 110	VL 111	RG 113	RG 115	RG 117	RG 118	RG 119	SB 120	SB 121	SB 122	SB 123	SB 124	SB 125	SB 126	SB 127	SB 128	SB 129	SB 131	SB 132	SB 133[a]	SB 133[b]
Th	0.950	0.69	–	1.20	–	0.42	–	2.79	0.57	0.91	–	4.24	–	4.12	–	2.10	–	–	3.48	3.91	0.72	3.34	–	2.28
U	0.398	0.292	–	0.482	–	0.189	–	0.862	0.255	0.352	–	1.34	–	1.31	–	0.746	–	–	1.03	1.04	0.342	0.934	–	0.774
La_N/Yb_N	4.70	3.10	–	4.60	–	2.10	–	11.6	2.40	3.40	–	15.5	–	13.8	–	7.70	–	–	10.1	7.10	2.80	10.8	–	8.10
Gd_N/Yb_N	1.30	1.20		1.20		1.00		1.80	1.00	1.00		2.20		2.00		1.20			1.40	1.50	1.10	1.70		1.30

bas. basalt, *b.a.* basaltic andesite, *and.* Andesite, *VL* Vella Lavella, *RG* Ranongga, *SB* Simbo

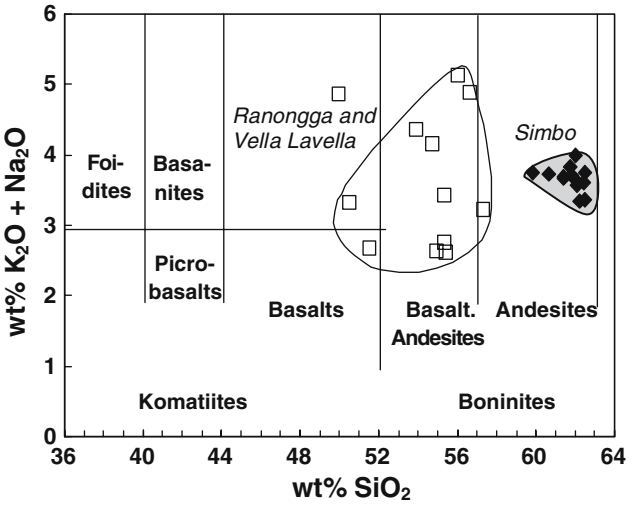

Fig. 3 TAS diagram (modified after Le Bas 2000) illustrating the division into two petrologic groups: Simbo-type andesites and Ranongga and Vella Lavella-type basalts and basaltic andesites. The group of Simbo-type andesites is shaded in *dark grey*; samples are shown as *filled diamonds*. Samples from Vella Lavella and Ranongga are marked by *open squares*. All data are recalculated volatile free

Discussion

General petrological classification of the analysed samples

Based on major and trace element compositions and geographical distribution of the samples, two suites can be discriminated. A group of basalts and basaltic andesites from Vella Lavella and Ranongga can be clearly distinguished from the group of more felsic opx-bearing HMA from Simbo. These HMA also occur in southernmost Ranongga (sample RG 117), which is geographically close to the Simbo Island. General enrichments in LREE and light lithophile elements (LILE) relative to high field strength elements (HFSE) in both suites (Fig. 5) and incompatible trace element systematics (Fig. 6) indicate a subduction-related setting and preclude an origin in a mid-ocean ridge setting. Hence, the petrogenesis of both suites along the across-arc traverse is related to subduction processes, even though the two groups were emplaced in a different tectonic position on opposite sides of the NBSC trench. Therefore it needs to be evaluated whether the HMA show affinities to boninites or, alternatively, are derived from slab melts that originate from old subducted oceanic crust.

Ranongga and Vella Lavella basalts and basaltic andesites

The Ranongga and Vella Lavella basalts and basaltic andesites display compositional features following

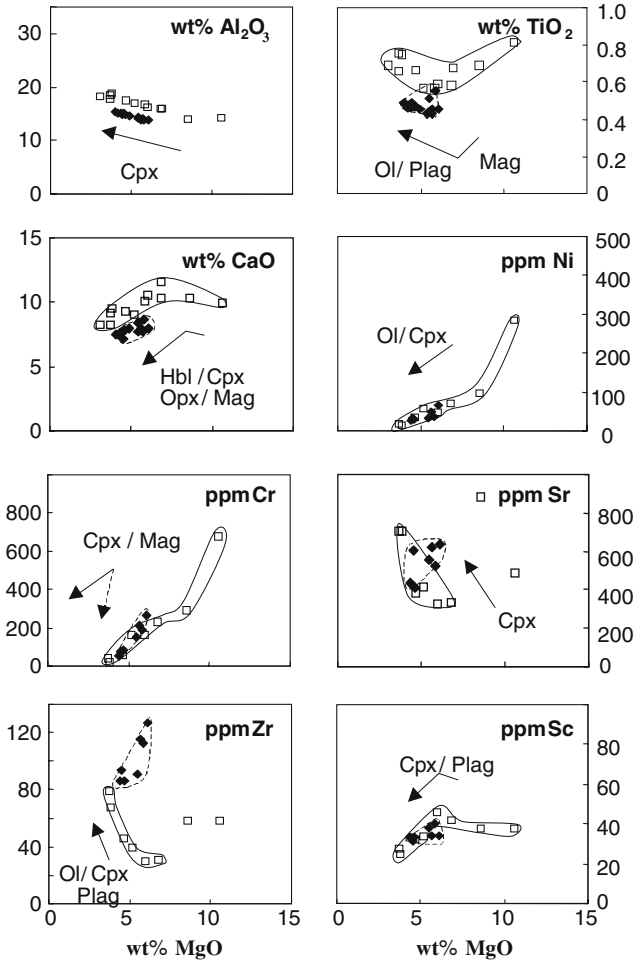

Fig. 4 Selected major and trace element variation diagrams for the Simbo-type andesites and Ranongga and Vella Lavella-type basalts and basaltic andesites (*symbols* are as in Fig. 3). *Vectors* indicate crystal fractionation trends. All data are recalculated volatile free

typical calc-alkaline fractionation trends, similar to basaltic magmas elsewhere in the Solomon arc (Schuth et al. 2004). Concentrations of K_2O, Na_2O, Al_2O_3 and Zr increase with decreasing MgO contents (Fig. 4). Concentrations of FeO, Cr and Ni, however, decrease. The samples with the highest MgO contents also display similar concentrations of compatible elements as primitive magmas. The observed range of compatible element concentrations indicates early fractionation of olivine from the parental magmas with the highest MgO content that most likely had basaltic compositions. At less than 8 wt% MgO, crystallization of clinopyroxene starts, as shown by decreasing CaO and Sc concentrations. As observed in many mafic island arc suites (e.g. Crawford et al. 1987), plagioclase fractionation is insignificant, as illustrated by increasing Al_2O_3 contents. The REE patterns of the Vella Lavella and Ranongga suite are mostly parallel, reflecting fractional crystallization from similar basaltic parent magmas. Small differences in $La_{(N)}/Yb_{(N)}$ ratios in this group, ranging from 1.4 to 4.6, can be explained by the fractionation of cpx and amphibole in which the LREEs have lower partition coefficients than the HREEs and MREEs (e.g. Hart and Dunn 1993). As observed in thin section, amphibole phenocrysts are restricted to samples VL 104 and VL 110 with $La_{(N)}/Yb_{(N)}$ = 4.6. As the HREEs are not depleted in the Vella Lavella and Ranongga suite, the magmas do originate from sources in the spinel lherzolite field (i.e. from depths not exceeding ca. 80 km). In summary, the parental magmas from Vella Lavella and Ranongga are similar to those in other present-day subduction-related settings.

Simbo-type magnesian andesites

Although located only less than 10 km south of Ranongga (Fig. 1), the petrological features of Simbo Island differ fundamentally from all other volcanic islands of the Solomon Islands. These specific features include the Mg-rich compositions, as indicated by the presence of orthopyroxene and disequilibrium olivine. Whereas the calc-alkaline volcanic rocks of the

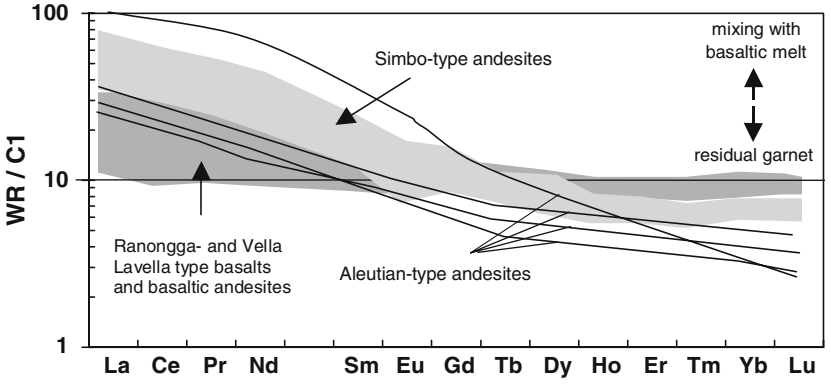

Fig. 5 Chondrite-normalized rare earth element patterns for the Simbo-type andesites and Ranongga and Vella Lavella-type basalts and basaltic andesites in comparison to representative Aleutian-type high magnesium andesites (Yogodzinski 1995). Normalization to CI is after Boynton (1984)

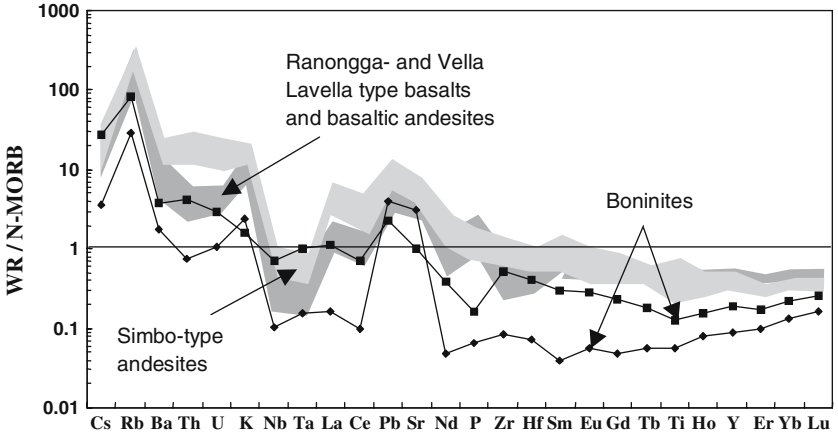

Fig. 6 N-MORB-normalized incompatible trace element diagram comparing the New Georgia basalts, basaltic andesites and the Simbo-type andesites with representative boninites from Cape Vogel, Papua New Guinea (*filled squares*, sample matrix glass 44264+ from Kamenetsky et al. 2002) and from Newfoundland (*filled diamonds*, sample BC-95 768 from Bédard 1999). N-MORB normalization values are after Hofmann (1988)

southern Solomon island chain were generated by melting of the hydrated mantle wedge above the subducting Indian–Australian plate (Petterson et al. 1999; Schuth et al. 2004), this process cannot account alone for the origin of the Simbo Island. As Simbo is located on a Woodlark Ridge transform fault south of the trench, MORB-like compositions would be expected. As the subduction-related incompatible trace element compositions of the Simbo rocks are distinctively different from patterns of typical back-arc basalts (Johnson et al. 1987, Fig. 6), the Simbo HMA cannot be derived from the adjacent Woodlark Ridge. In order to account for magmatism on Simbo, the presence of subduction components is required in the magma sources. As indicated by Pb isotope compositions of the Simbo HMA (Fig. 11), an important source of the subduction components is probably the Pacific plate, which was subducted beneath the Solomon Islands in Eocene time (Petterson et al. 1999, Mann and Taira 2004). The unusual tectonic setting of Simbo is also reflected in the geochemistry of the andesites. Simbo

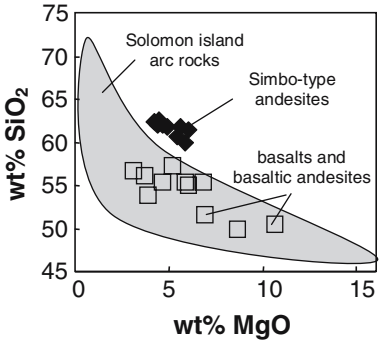

Fig. 7 SiO_2–MgO plot for Simbo-type andesites in comparison to the basalts and basaltic andesites from Vella Lavella and Ranongga and to volcanic rocks from other islands of the Solomon arc (*shaded field*, data from Schuth et al. 2004 and personal communication)

rocks are much more enriched in MgO and Ni–Cr for a given SiO_2 composition (Fig. 7). Additionally, the high Mg# of Simbo-volcanic rocks overlaps with those of primitive magmas (Mg# > 65). As boninites also display such high MgO contents (e.g. Crawford et al. 1989), their possible petrogenetic role for Simbo-type magmatism is discussed below.

A boninitic source of Simbo-type magmas?

Boninites are characterized by MgO contents of more than 8 wt%, above 52 wt% SiO_2 and less than 0.5 wt% TiO_2 (Le Bas 2000). They are derived from a refractory, peridotitic source that is enriched by hydrous fluids that lower the solidus. Estimated melting temperatures for boninites lie between 1,100 and 1,150°C (e.g. Sun and Nesbitt 1978; Crawford et al. 1981; Tatsumi 1982; Hickey and Frey 1982; Cameron et al. 1983; Bloomer and Hawkins 1987; Beccaluva and Serri 1988). In order to generate boninitic melts, the combined effects of intense hydration and an elevated temperature gradient trigger re-melting of the refractory mantle sources. Among various tectonic settings, boninitic melts are frequently generated in forearc environments at relatively shallow depths (ca. 50–30 km; Crawford et al. 1989) where unusually hot oceanic crust is subducted, similar to the tectonic setting beneath the Solomon Islands. Such forearc-related boninites occur at the Bonin Islands (Kikuchi 1890; Petersen 1891), the Marianas (Dietrich et al. 1978), the Lau Basin (Hawkins 1995), New Caledonia (Koh Ophiolith, Meffre et al. 1996) and Papua New Guinea (Dallwitz et al. 1966; Jenner 1981) in the western Pacific. Olivine phenocrysts in boninites typically range from Fo_{88} to Fo_{94} in composition, often show some evidence for resorption and can be surrounded by clinoenstatite (Jenner 1981; Walker and Cameron 1983). A striking feature of boninites is their concave

(U-shaped) REE patterns (e.g. Jenner 1981; Hickey and Frey 1982; Cameron et al. 1983). These patterns are interpreted to indicate the addition of a LREE-enriched component to the refractory peridotite source prior to or during boninite melting (e.g. Crawford et al. 1981; Cameron et al. 1983; Meffre et al. 1996).

As indicated by comparison to other boninite occurrences, the presence of boninites can be expected in the Solomon arc because (1) the arc chain is located very close to the NBSC trench and (2) very young and hot oceanic crust is subducted. However, as illustrated above, Simbo Island is not located in the forearc region, but is located on the subducting Indian–Australian plate. It is therefore not surprising that the major and trace element features of the Simbo magnesian andesites do not match compositions of true boninites. In contrast to true boninites, Simbo-type rocks display lower MgO contents at given SiO_2 contents (4–6 wt% MgO compared to a minimum of 8 wt% MgO in boninites). It is also difficult to explain the compositions of the Simbo andesites by crystal fractionation from boninitic parental magmas, because the Simbo magmas display nearly primitive Mg# (67–75). Moreover, the Simbo andesites do not display characteristic concave incompatible trace element patterns and are not as depleted in incompatible elements as typical boninites (Fig. 6). In conclusion, a boninitic origin can therefore be ruled out for the Simbo HMA.

Evidence for the role of slab melts

Other andesites with similarly high MgO contents and HREE depletions as the Simbo rocks are slab melt-related HMA that also occur in island arc regimes. While slab melt-related HMA are not strictly defined with respect to their geochemical characteristics, their petrogenesis involves different processes than those generating boninites. These HMA (i.e. adakites) originate from the interaction of slab melts with the overlying mantle wedge and typically exhibit a silicic endmember that is attributed to partial melting of subducted eclogitic crust (Kay 1978, 1980; Stern and Kilian 1996). In contrast to experimental prediction (e.g. Rapp and Watson 1995), modern adakites display higher MgO contents (e.g. Martin 1986), reflecting mixing with mantle material (Yogodzinski 1995). Such mixtures display trace element compositions that are transitional between adakites and more typical island arc andesites, e.g. Sr/Y ratios less than 100 but still higher than typical arc andesites (< 30). Sr/Y ratios in the Simbo HMA are similar to those in other HMA occurrences. Such occurrences include the New Hebrides (e.g. Monzier et al. 1993), the Aleutians (e.g. Yogodzinski 1995), Kamchatka (e.g. Kepezhinskas et al. 1995; Yogodzinski et al. 2001), the Cascades (e.g. Grove et al. 2002) and the Andean Austral volcanic zone in South America (e.g. Stern and Kilian 1996). Collectively, the major and trace element evidence indicates that slab melts appear to play an important role during the petrogenesis of the Simbo andesites.

The Simbo-type rocks display a clear depletion in HREE compared to MORB and volcanic rocks from Vella Lavella and Ranongga (Figs. 5, 6). The depletion in HREE relative to MREE is indicated by $Gd_{(N)}/Yb_{(N)}$ values which range from 1.3 to 2.2 ($La_{(N)}/Yb_{(N)}$ = 5.2–10.4), clearly above values of 1.0–1.3 ($La_{(N)}/Yb_{(N)}$ = 1.4–3.2) for the Ranongga and Vella Lavella suite (Table 4). The HREE depletion in the Simbo andesites together with the silicic composition of the rocks points to subducted eclogitic crust as one source of the Simbo andesites (e.g. Martin 1986; Rapp and Watson 1995). Residual garnet in the mantle source (e.g. $D^{Gr/L}Yb$ = 3.9; Hauri et al. 1994) buffered the HREE in the Simbo andesites. Martin (1986) and Defant and Drummond (1990) use bulk REE fractionation $La_{(N)}/Yb_{(N)}$ and Sr/Y to distinguish between pristine adakites and typical island arc volcanic rocks. Using these criteria, Simbo-type rocks as well as sample RG 117 from southern Ranongga (Sr/Y from 30 to 53) plot at the lower end of the adakite fields, but clearly outside the field for typical island arc rocks (Fig. 8a, b).

Ascending adakitic melts can mix with either mantle peridotite or other mafic melts at variable proportions which results in an ''overprint'' of pristine adakitic signatures, thus lowering initially high $Gd_{(N)}/Yb_{(N)}$ ratios (Yogodzinski 1995; Stern and Kilian 1996; Kelemen et al. 1993). In Fig. 5, a comparison of REE patterns of Simbo-type andesites and a suite of variably ''overprinted'' adakitic REE patterns of HMA from the Aleutians is shown. In comparison to the Aleutian rocks, Simbo andesites plot at the upper end with respect to the HREE depletion. The somewhat intermediate HREE depletion confirms the admixture of a mafic component to pristine adakitic melts. Given the plate tectonic setting of the Simbo andesites, this mafic component is most likely mantle wedge peridotite beneath the Indian–Australian plate or Woodlark-type basalt. Elevated MgO contents are another indicator for adakite–mantle wedge interaction (Sen and Dunn 1994; Sajona 1995; Maury et al. 1996). This feature is also evident for the Simbo andesites that display MgO contents from 4 to 6 wt%, overlapping with the upper MgO range in typical adakites.

As a first conclusion, Simbo-type andesites show geochemical characteristics similar to adakites and,

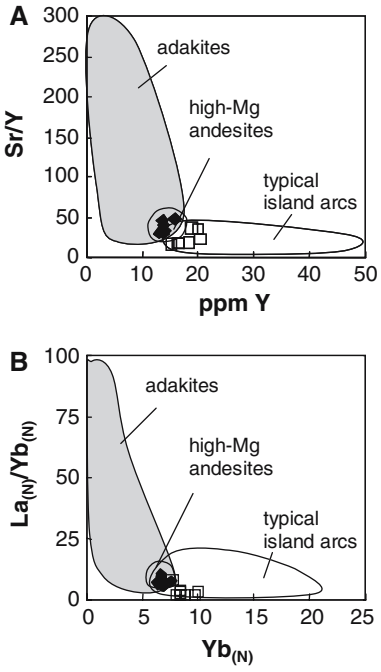

Fig. 8 Diagrams discriminating between adakitic (*grey fields*) and typical calc-alkaline arc compositions (*white fields*), showing the compositions of the Simbo-type high-Mg andesites. **a** Sr/Y versus Y (Defant and Drummond 1990). **b** $La_{(N)}/Yb_{(N)}$ versus $Yb_{(N)}$ (Martin 1986)

even though falling short of matching the exact adakite definition, they clearly exhibit slab melt signatures. The presence of slab melts with steep REE patterns requires the presence of a subducted eclogitic plate beneath Simbo. A likely source is the fossil slab of Pacific oceanic crust that was subducted beneath the Solomon Islands until 20 Ma ago (Petterson et al. 1999). In order to elucidate the source of the slab melts closer, isotope systematics are used below. This approach, however, requires the identification of the mafic mixing endmember first.

Evidence for binary mixing and identification of a potential mafic endmember

A characteristic feature of the Simbo andesites is olivine xenocrysts that are surrounded by orthopyroxenes (Fig. 2a). Hence, an olivine-bearing mafic component was admixed to a relatively SiO_2-rich slab-derived melt. Nickel concentrations in olivine and orthopyroxene from Simbo-type andesites support this scenario (Fig. 2b). Olivine bearing peridotite or -basalts, similar to those erupted along the adjacent Woodlark Ridge (Johnson et al. 1987), may represent suitable mafic endmembers. Mantle peridotite has previously been considered as mafic endmember in the petrogenesis of arc rocks that involve slab melting (Martin 1986; Yogodzinski 1995). The mantle sources of Woodlark Ridge basalts are slightly overprinted by subduction components (Johnson et al. 1987; Perfit et al. 1987) as they are located in a back-arc position to the northeastern Solomon island chain where volcanism was triggered by the subduction of the Pacific beneath the Indian–Australian plate. The measured olivine compositions in the Simbo andesites ($Fo_{88–90}$) do not enable a discrimination between peridotite and basalts as they overlap with values found in both primitive basalts and peridotites (Sobolev et al. 2005). In order to discriminate between the two possible

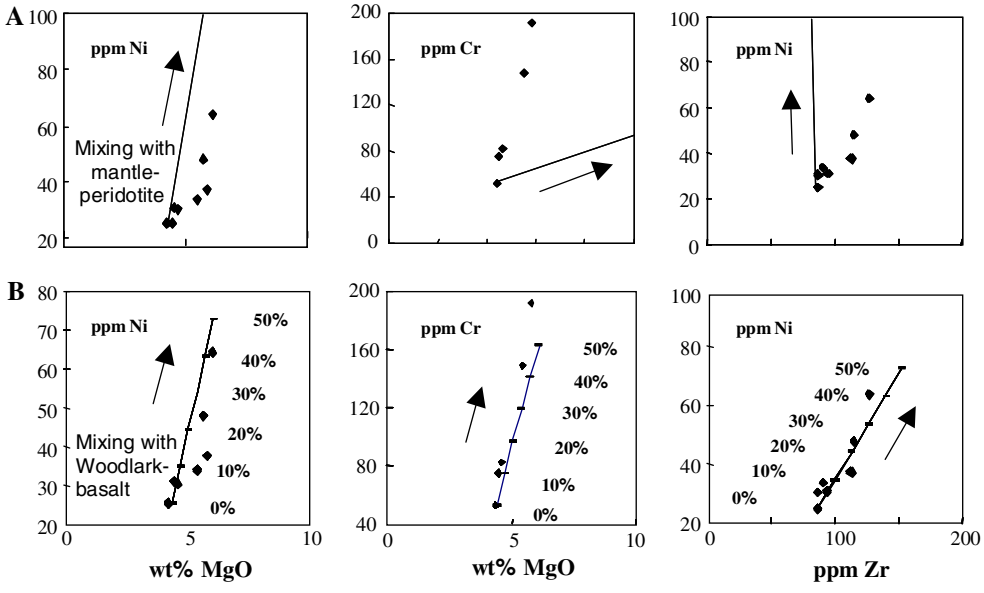

Fig. 9 Mixing models explaining the petrogenesis of Simbo-type andesites (*filled diamonds*) by mixing of adakitic melts with potential mafic endmembers. **a** Mantle peridotite as mafic endmember (data from Workman and Hart 2004). **b** Typical basalt from the Woodlark Ridge (samples KAK-820316-032-15(G)*, –029-018+, data from Perfit et al. 1987) as mafic endmember. Mixing lines with Woodlark-type basalt are labelled with *percentages*. The compositions of the Simbo andesites are difficult to reconcile with simple admixture of mantle peridotite

mafic endmembers, mixing curves of a typical adakitic melt with both possible endmembers were calculated (Fig. 9). As shown in Fig. 9a, admixture of olivine-bearing peridotite alone is unlikely to account for the Cr-, Ni- and MgO contents in the Simbo-type rocks. Even if a large uncertainty in the peridotite composition is assumed, the initial concentrations of Cr, Ni and MgO in the peridotites are still too high and would result in higher bulk concentrations than observed in the Simbo andesites. Minor additions of peridotite and more complex chromatographic interactions with peridotite (rather than mixing), however, cannot unequivocally be ruled out using such a simplified mixing model.

In contrast to a peridotite-mixing scenario, the mixing calculations are clearly consistent with a basaltic mixing endmember, similar to basalts from the Woodlark Ridge (Fig. 8b). The model requires the addition of up to 50% Woodlark-type basalt to the adakitic melts in order to yield as much as 6 wt% MgO in the Simbo andesites. This estimate, however, strongly depends on the MgO content that is assumed for the Woodlark basalt (an average of ca. 8 wt% MgO has been used here; Perfit et al. 1987). A slightly higher MgO concentration in the Woodlark basalt component would require lower amounts of added basaltic melt. As for MgO, the Cr and Ni mass balance strongly depends on the estimated average composition of the basaltic endmember. Assuming average basaltic compositions, 40–50% of Woodlark-type basalt can explain the Ni and Cr compositions of the Simbo andesites. The addition of back-arc type basalts to the felsic melts is also supported by a rather unusual positive correlation between MgO contents and Zr abundances in the Simbo andesites (Fig. 4). Such a positive correlation requires the Zr concentrations in the mafic component to be higher than those in the adakitic component. Indeed, such elevated Zr concentrations (above 100 ppm) are typically found in MORB and back-arc basalts like those in the Woodlark basin (Johnson et al. 1987; Perfit et al. 1987).

In conclusion, a binary mixture between a slab-derived melt and a mafic melt is indicated by olivine xenocrysts with reaction-rims of opx, as well as by high MgO, Ni and Cr contents that are unusually high for andesitic rocks. A mixing model supports Woodlark-type basaltic melts as the potential mafic endmember. Admixture of mantle peridotite requires more complex chromatographic mechanisms. The primitive xenocrystic olivines are most likely liquidus olivines that already crystallized from these mafic melts. The admixture of basaltic melts also explains the relatively small depletion of HREE in the Simbo-type andesites, compared to typical adakites. This observation is similar to those in other adakite occurrences (Sen and Dunn 1994; Sajona 1995; Maury et al. 1996).

Isotope constraints on the sources of the two magmatic groups

The Sr–Nd isotope compositions of the two rock groups are similar to that of all other rocks analysed so far from the New Georgia group (Schuth et al. 2004) and are also close to those of the adjacent New Britain and Vanuatu arcs (Fig. 10a). Previous workers (Hickey-Vargas et al. 1995; Schuth et al. 2004) argued that a relict Indian-type mantle wedge is still present beneath the Solomon Islands that originates from the Eocene–Miocene subduction of the Pacific plate beneath the Indian–Australian plate. The isolation of the relict Indian-type mantle domain occurred when subduction polarity switched to its present day northward direction. Compared to all other islands of the Solomon group, the Simbo Island is the only active subaerial volcano that is located on the Indian–Australian plate

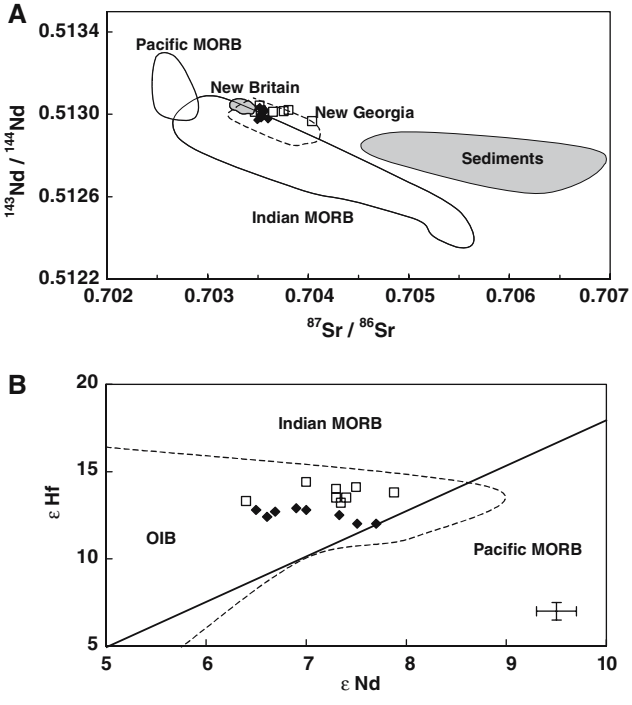

Fig. 10 **a** Comparison of Sr–Nd isotope values obtained for the western New Georgia samples with those of other SW-Pacific arc rocks. Vanuata data are from Peate et al. (1997), sediment and New Britain data from Woodhead et al. (1998), Pacific and Indian MORB fields are after Hofmann (1997), New Georgia field is after Schuth et al. (2004). **b** εNd–εHf plot. The *thick line* represents the discrimination line between Indian and Pacific MORB, modified after Kempton et al. (2002). *Symbols* are as in Fig. 3

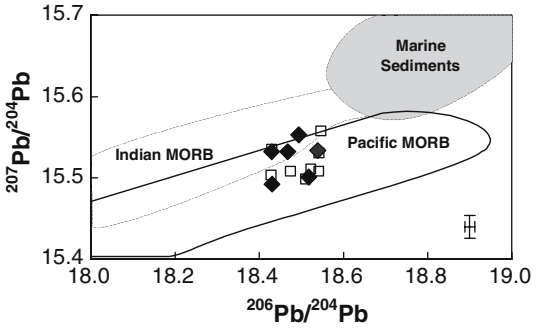

Fig. 11 Pb isotope compositions of the analysed samples. Fields after Peate et al. (1997)

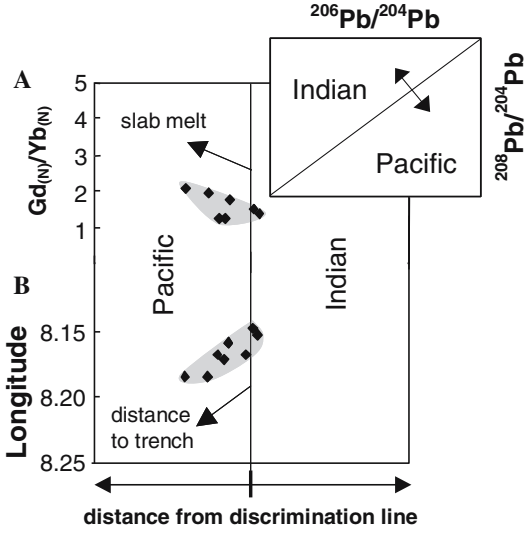

Fig. 12 **a** Plot of $Gd_{(N)}/Yb_{(N)}$ as indicator for slab melt signature versus Pb isotope discrimination parameter (DDL) between Indian and Pacific Pb isotope compositions. The *vector* indicates the shift towards an increasingly Pacific Pb isotope composition with increasing slab melt components. **b** Longitude (degree south) versus Pb isotope discrimination parameter (DDL). The *vector* indicates an increasingly Pacific Pb isotope composition with greater distance to the San Cristobál trench toward the south. DDL is calculated as discrimination score after Kempton et al. (2002):$(-18.109 \times {}^{206}Pb/{}^{204}Pb) + (12.950 \times {}^{208}Pb/{}^{204}Pb)$

and is separated from the adjacent islands of Ranongga and Vella Lavella by the presently active NBSC trench to the north (Fig. 1; e.g. Yoneshima et al. 2005).

In the SW-Pacific realm, combined Hf–Nd isotope systematics in oceanic basalts have proven useful to discriminate between Pacific and Indian–Australian type mantle domains (e.g. Kempton et al. 2002; Pearce et al. 1999; Schuth et al. 2004). The new Hf–Nd isotope data suggest that the sources of all three volcanic islands are part of the Indian–Australian mantle domain (Fig. 10b). Interestingly, Simbo-type rocks systematically display slightly lower εHf values than rocks from Ranongga and Vella Lavella. Such across-arc shifts in Hf isotope signatures have previously been reported for other western Pacific arcs (Woodhead et al. 2001). In the case of Simbo, the across-arc transition to lower εHf values probably reflects regional variations in the Indian domain that are now juxtaposed by Phanerozoic subduction processes or, alternatively, possible differences in εHf between the Indian and Pacific endmembers.

In conjunction with Hf–Nd isotope systematics, Pb isotope compositions of arc rocks are also sensitive tracer for subducted sediments. Moreover, Pb isotope compositions are also significantly different between the Indian–Australian and Pacific mantle domains (e.g. Kempton et al. 2002). As Pb behaves highly mobile in subduction systems (e.g. Chauvel et al. 1995), Pb isotope compositions may help to unravel the source of subduction components that are derived from oceanic crust. Because $^{207}Pb/^{204}Pb$ compositions of the analysed samples overlap with those of MORB (Fig. 11), any significant addition of subducted pelagic sediments to the magma sources can be ruled out. However, a significant influence of subduction components derived from the older subducted Pacific slab on the compositions of all volcanic rocks, including Simbo-type andesites, is revealed (Fig. 12). This observation is confirmed by geophysical data which indicate the presence of a fossil slab of Pacific oceanic crust at depths of up to 160 km beneath the region examined here (Mann et al. 1998). Such depths are within the eclogite stability field but above the supercritical point of slab-derived fluids and melts (Kessel et al. 2005), thus arguing for the presence of adakitic melts. Hence, both isotopic and geophysical data point towards the presence of HREE-depleted adakitic melts that are derived from the subducted Pacific plate. This model is furthermore supported by coupled Pb isotope and HREE variations. Samples with the most pronounced Pacific Pb isotope composition also display the most prominent slab melt signature (high $Gd_{(N)}/Yb_{(N)}$, Fig. 12a). The slab melt contributions increase with distance from the NBSC trench (Fig. 12b).

In Fig. 13a, a projection of $\Delta\varepsilon Nd_{P/I}$ versus ΔNd after Pearce et al. (1999) is shown. The $\Delta\varepsilon Nd_{P/I}$ parameter is the deviation of a sample from the Pacific–Indian discrimination line in Hf–Nd isotope space. ΔNd denotes the enrichment of Nd relative to Hf by subduction components. In agreement with Pb isotope compositions, constant $\Delta\varepsilon Nd_{P/I}$ with increasing ΔNd rule out the addition of significant amounts of pelagic sediments (unradiogenic Nd) to the sources of all rock groups. Rather, additions of components derived from Pacific MORB and from subducted volcanic sediment are indicated, the latter probably resulting from high uplift and erosion rates close to the trench (Mann et al.

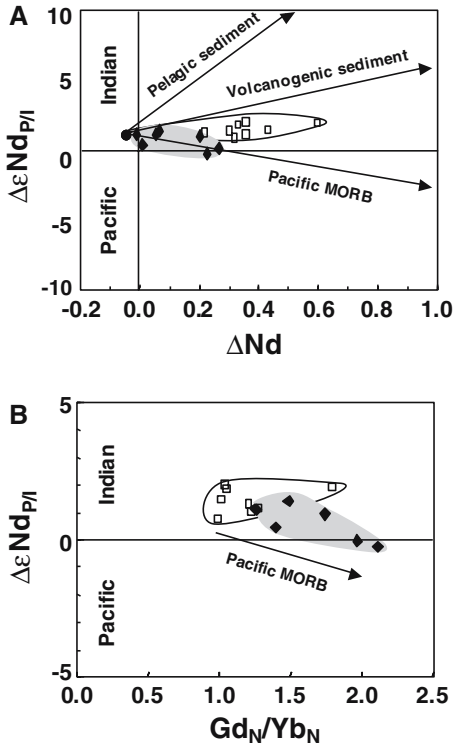

Fig. 13 **a** $\Delta\varepsilon Nd_{P/I}$ versus ΔNd projection for the Simbo-type andesites and RVBB. *Vectors* indicate addition of fluids/melts derived from subducted pelagic/volcanogenic sediment and components derived from Pacific MORB and are taken from Pearce et al. (1999). $\Delta\varepsilon Nd_{P/I}$ is calculated relative to the Pacific/Indian mantle domain discrimination line of Pearce et al. (1999). Equations are: $\Delta\varepsilon Nd_{P/I} = 0.625\varepsilon Hf - \varepsilon Nd$ and $\Delta\varepsilon Nd_{P/I} = [(Nd/Yb) - 10^{(0.674+1.414\log(Hf/Yb))}]/[Nd/Yb]$. **b** $\Delta\varepsilon Nd_{P/I}$ versus $Gd_{(N)}/Yb_{(N)}$, illustrating the increasingly Pacific Hf–Nd signature in the Simbo samples with increasing slab melt contribution

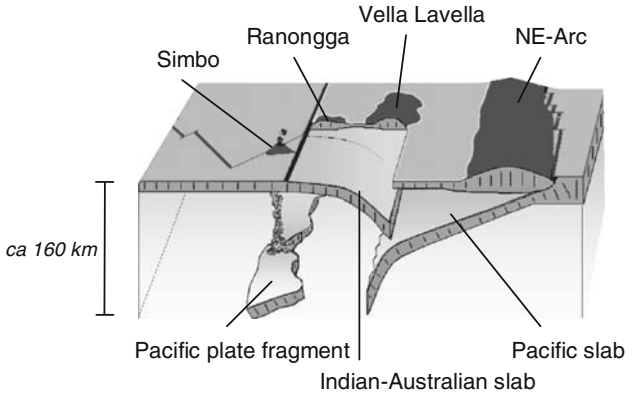

Fig. 14 Schematic sketch, illustrating the proposed petrogenetic model for the Simbo-type andesites and the basalts/basaltic andesites from Vella Lavella and Ranongga. As confirmed by geophysical evidence, the slab melt component in the Simbo high-magnesium andesites originates from a detached part of the fossil Pacific plate that was subducted until Miocene time. Depth of detached plate fragment is ca. 160 km

1998). In $\Delta\varepsilon Nd_{P/I}$ versus ΔNd space, Simbo-type andesites show a characteristic shift towards compositions of subducted Pacific MORB. This reflects the increasing influence of slab-derived melts from the subducted Pacific plate (Fig. 13b) and is consistent with the observations above. A schematic plate tectonic sketch summarizing the petrogenesis of Simbo andesites and the basalts and basaltic andesites from Ranongga and Vella Lavella is shown in Fig. 14.

Conclusion

On the basis of geochemical and petrological data obtained for volcanic rocks from the western part of the New Georgia archipelago, a group of magnesian andesites from the island of Simbo on the Indian–Australian plate can be distinguished from a basaltic and basaltic andesitic group from the islands of Vella Lavella and Ranongga that are located on the Pacific plate and are separated from Simbo by the NBSC trench.

Compositions of the Simbo-type magnesian andesites are unique among all other analysed samples from the Solomon Island region. The trace element composition of the Simbo andesites is partially inherited from slab-derived melts that originate from a fossil slab of subducted Pacific oceanic crust. Reaction of the ascending slab melts with basaltic melts and possibly with mantle peridotite has resulted in a dilution of the pristine adakitic melts and has modified the initially HREE-depleted REE patterns. The basaltic end-member is most likely back-arc-type basalt from the Woodlark Ridge. During reaction with the basaltic component, the ascending silicic slab melt assimilated olivine phenocrysts.

Lead isotope compositions reveal the influence of subduction components derived from the older subducted Pacific plate on magma compositions on all three islands. Indian-type Pb isotope signatures are restricted to samples from southern Ranongga and the northernmost part of Simbo. Both areas are located closest to the presently active NBSC trench, where lower amounts of Pacific subduction components appear to be present, as also shown by decreasing slab melt signatures in these samples. Coupled Hf–Nd isotope relationships reveal the presence of the Indian–Australian type mantle domain beneath Simbo. Moreover, a relict wedge of Indian–Australian type mantle underlies the islands presently located on the Pacific plate as already shown by previous studies (Schuth et al. 2004). Displacements towards Pacific Hf–Nd isotope signatures in Simbo-type magnesian

andesites are most pronounced in samples with the highest slab melt component. This clearly demonstrates the overprint of pristine Indian–Australian type Hf–Nd isotope signatures by Pacific signatures.

High geothermal gradients that are required for slab melting are provided by the subduction of the Woodlark spreading centre and also by the disruption of the Pacific slab that was previously suggested by Petterson et al. (1999), possibly leading to rapid heating along torn slab edges. This scenario is analogous to similar settings in Central America or Kamchatka (Abratis and Wörner 2001; Yogodzinski et al. 2001). In addition to the steep geothermal gradients in the region, the presence of a transform fault beneath Simbo facilitates the ascent of slab melts.

Acknowledgments This research was supported by the DFG (German Research Foundation, project MU 1406/2–3). Heidi Baier and Jasper Berndt are thanked for lab support. We thank Radegund Hoffbauer from Universität Bonn for XRF analyses and Dieter Garbe-Schönberg from Universität Kiel for quadrupole ICP-MS analyses. Andrew Mason and Stanley Basi provided support in organizing the field campaign in the Solomon Islands. Journal reviews by two anonymous reviewers helped to improve the manuscript.

References

Abraham DA, Backisapa M, Booth DJ, Dunkley PN, Hughes GW, Langford RL, Philip PR, Ridgway J, Smith A, Strange PJ (1987) New Georgia group geological map sheet, 1:250.000. Geological Survey Division, Ministry of Natural Resources, Honiara, Solomon Islands

Abratis M, Wörner G (2001) Ridge collision, slab-window formation, and the flux of Pacific asthenosphere into the Caribbean realm. Geology 29:127–130

Beccaluva L, Serri G (1988) Boninitic and low-Ti subduction-related lavas from intraoceanic arc backarc systems and low-Ti ophiolites—a reappraisal of their petrogenesis and original tectonic setting. Tectonophysics 146:291–315

Bédard JH (1999) Petrogenesis of boninites from the Betts Cove Ophiolite, Newfoundland, Canada: identification of subducted source components. J Petrol 40:1853–1889

Bindeman IN, Eiler JM, Yogodzinski GM, Tatsumi Y, Stern CR, Grove TL, Portnyagin M, Hoernle K, Danyushevsky LV (2005) Oxygen isotope evidence for slab melting in modern and ancient subduction zones. Earth Planet Sci Lett 235:480–496

Blichert-Toft J, Albaréde F (1997) The Lu–Hf isotope geochemistry of chondrites and the evolution of the mantle–crust system. Earth Planet Sci Lett 148:243–258

Bloomer SH, Hawkins JW (1987) Petrology and geochemistry of boninite series volcanic rocks from the Mariana trench. Contrib Mineral Petrol 97:361–377

Boynton WV (1984) Cosmochemistry of the rare earth elements: meteorite studies. In: Henderson P (ed) Rare earth element geochemistry. Elsevier, Amsterdam, pp 89–94

Brown GM, Schairer JF (1968) Melting relations of some calcalkaline volcanic rocks. Carnegie Inst Wash Yearb 66:460–467

Cameron WE, McCulloch MT, Walker DA (1983) Boninite petrogenesis: chemical and Sr–Nd isotopic constraints. Earth Planet Sci Lett 65:75–89

Chauvel C, Goldstein SL, Hofmann AW (1995) Hydration and dehydration of oceanic crust controls Pb evolution in the mantle. Chem Geol 126:65–75

Cowley S, Mann P, Coffin MF, Shipley T (2004) Oligocene to recent tectonic history of the central Solomon intra-arc basin as determined from marine seismic reflection data and compilation of onland geology. Tectonophysics 389:267–307

Crawford AJ, Beccaluva L, Serri G (1981) Tectono-magmatic evolution of the west Philippine-Mariana region and the origin of boninites. Earth Planet Sci Lett 54:346–356

Crawford AJ, Falloon TJ, Eggins S (1987) The origin of high-alumina basalts. Contrib Mineral Petrol 97:417–430

Crawford AJ, Falloon TJ, Green DH (1989) Classification, petrogenesis and tectonic setting of boninites. In: Crawford AJ (ed) Boninites and related rocks. Unwin Hyman, Boston, pp 2–49

Dallwitz WB, Green DH, Thompson JE (1966) Clinoenstatite in a volcanic rock from the Cape Vogel area, Papua. J Petrol 7:75–403

Defant MJ, Drummond MS (1990) Derivation of some modern arc magmas by melting of young subducted lithosphere. Nature 347:662–665

Defant MJ, Drummond MS (1993) Mount St. Helens—potential example of the partial melting of the subducted lithosphere in a volcanic arc. Geology 21:574–550

Dietrich V, Emmermann R, Oberhänsli R, Puchelt H (1978) Geochemistry of basaltic and gabbroic rocks from the West Mariana basin and the Mariana trench. Earth Planet Sci Lett 39:127–144

Gill J (1981) Orogenic andesites and plate tectonics. Springer, Berlin Heidelberg New York, p 390

Gill J, Compston W (1973) Strontium isotopes in island arc volcanic rocks. In: Coleman PJ (ed) The western Pacific: island arcs, marginal seas. Geochemistry, pp 83–494

Govindaraju K (1994) 1994 compilation of working values and sample description for 383 geostandards. Geostand Newsl 18:1–158

Grove TL, Parman SW, Bowring SA, Price RC, Baker MB (2002) The role of an H_2O-rich component in the generation of primitive basaltic andesites and andesites from the Mt. Shasta region, N. California. Contrib Mineral Petrol 142:375–396

Hart SR, Dunn T (1993) Experimental cpx/melt partitioning of 24 trace elements. Contrib Mineral Petrol 113:1–8

Hauri EH, Wagner TP, Grove TL (1994) Experimental and natural partitioning of Th, U, Pb and other trace elements between garnet, clinopyroxene and basaltic melts. Chem Geol 117:149–166

Hawkins J (1995) Evolution of the Lau Basin—insights from ODP Leg 135—active margins and marginal basins of the western Pacific. Geophys Monogr 88:125–173

Heinrichs H, Herrmann AG (1990) Praktikum der analytischen Geochemie. Springer, Berlin Heidelberg New York, p 667

Hickey RL, Frey FA (1982) Geochemical characteristics of boninite series volcanics: implications for their source. Geochim Cosmochim Acta 46:2099–2115

Hickey-Vargas R, Hergt JM, Spadea P (1995) The Indian ocean-type isotopic signature in western Pacific marginal basins: origin and significance. In: Taylor B, Natland JP (eds) Active margins and marginal basins of the Western Pacific. Geophys Monogr Am Geophys Union, vol 88, pp 175–197

Hofmann AW (1997) Mantle geochemistry: the message from oceanic volcanism. Nature 385:219–229

Hussong DM, Wipperman LK, Kroenke LW (1979) The crustal structure of the Ontong Java and Manihiki oceanic plateaus. J Geophys Res 84:6003–6010

Ionov DA, Griffin WL, O'Reilly SY (1997) Volatile-bearing minerals and lithophile trace elements in the upper mantle. Chem Geol 141:153–184

Jacobsen SB, Wasserburg GJ (1980) Sm–Nd isotopic evolution of chondrites. Earth Planet Sci Lett 50:139–155

Jenner GA (1981) Geochemistry of high-Mg andesites from Cape Vogel, Papua New Guinea. Chem Geol 33:307–332

Johnson RW, Jaques AL, Langmuir CH, Perfit MR, Staudigel H, Dunkley PN, Chappell BW, Taylor SR, Baekisapa M (1987) Ridge subduction and forearc volcanism: Petrology and geochemistry of rocks dredged from the western Solomon arc and Woodlark basin. Circum-Pac Counc Energy Miner Res 7:155–226

Kamenetsky VS, Crawford AJ, Eggins S, Mühe R (1997) Phenocryst and melt inclusion chemistry of near-axis seamounts, Valu Fa Ridge, Lau Basin: insight into mantle wedge melting and the addition of subduction components. Earth Planet Sci Lett 151:205–223

Kamenetsky VS, Sobolev AV, Eggins SM, Crawford AJ, Arculus RJ (2002) Olivine-enriched melt inclusions in chromites from low-Ca boninites, Cape Vogel, Papua New Guinea: evidence for ultramafic primary magma, refractory mantle source and enriched components. Chem Geol 183:287–303

Kay RW (1978) Aleutian magnesian andesites: melts from subducted Pacific ocean crust. J Volcanol Geotherm Res 4:117–132

Kay RW (1980) Volcanic arc magmas: implications of a melting-mixing model for element recycling in the crust–upper mantle system. J Geol 88:497–522

Kelemen PB, Shimizu N, Dunn T (1993) Relative depletion of niobium in some arc magmas and the continental crust—partitioning of K, Nb, La and Ce during melt/rock reaction in the upper mantle. Earth Planet Sci Lett 120:111–134

Kelemen PB, Rilling JL, Parmentier EM, Mehl L, Hacker BR (2003) Thermal structure due to solid-state flow in the mantle wedge beneath arcs. In: Eiler JM (ed) Inside the subduction factory. AGU, Washington, pp 293–311

Kempton PD, Pearce JA, Barry TL (2002) Sr–Nd–Pb–Hf isotope results from ODP Leg 187: evidence for mantle dynamics of the Australian–Antarctic Discordance and origin of the Indian MORB source. Geochem Geophys Geosyst 3, paper no. 10.1029/2002GC000320

Kepezhinskas PK, Defant MJ, Drummond MS (1995) Na metasomatism in the island-arc mantle by slab melt–peridotite interaction: evidence from mantle xenoliths in the North Kamchatka arc. J Petrol 36:1505–1527

Kessel R, Schmidt MW, Ulmer P, Pettke T (2005) Trace element signature of subduction-zone fluids, melts and supercritical liquids at 120–180 km depth. Nature 437:724–727

Kikuchi Y (1890) On pyroxene components in certain volcanic rocks from bonin island. J Coll Sci Imp Univ Jpn 3:67–89

Klemme S (2004) The influence of Cr on the garnet-spinel transition in the Earth's mantle: experiments in the system $MgO–Cr_2O_3–SiO_2$ and thermodynamic modelling. Lithos 77:639–646

Le Bas MJ (2000) IUGS reclassification of the high-Mg and picritic volcanic rocks. J Petrol 41:1467–1470

Mann P (1997) Model for the formation of large transtensional basins in zones of tectonic escape. Geology 25:211–214

Mann P, Taira A (2004) Global tectonic significance of the Solomon Islands and Ontong Java Plateau convergent zone. Tectonophysics 389:137–190

Mann P, Taylor WF, Lagoe MB, Quarles A, Burr G (1998) Accelerating late Quaternary uplift of the New Georgia Island group (Solomon Islands arc) in response to subduction of the recently active Woodlark spreading center and Coleman seamount. Tectonophysics 295:259–306

Marshak RS, Karig DE (1977) Triple junctions as a cause for anomalously near trench activity between the trench and volcanic arc. Geology 5:233–236

Martin H (1986) Effect of steeper Archaeach geothermal gradient on geochemistry of subduction-zone magmas. Geology 14:753–756

Martin H, Moyen JF (2002) Secular changes in tonalite-trondhjemite-granodiorite composition as markers of the progressive cooling Earth. Geology 30:319–322

Maury RC, Sajona FG, Pubellier M, Bellon H, Defant MJ (1996) Fusion de la croÛte océanique dans les zones de subduction/collision récentes: l'exemple de Mindano (Philippines). Bull Soc Geol (Fr) 167:579–595

McCulloch MT, Gamble JA (1991) Geochemical and geodynamical constraints on subduction zone magmatism. Earth Planet Sci Lett 102:358–374

Meffre S, Aitchison JC, Crawford AJ (1996) Geochemical evolution and tectonic significance of boninites and tholeiites from the Koh ophiolite, New Caledonia. Tectonics 15:67–83

Miura S, Kodaira S, Nakanishi A, Tsuru T, Takahashi N, Hirata N, Kaneda Y (2003) Structural characteristics controlling the seismicity crustal structure of southern Japan trench fore-arc region, revealed by ocean bottom seismographic data. Tectonophysics 363:79–102

Monzier M, Danyushevsky LV, Crawford AJ, Bellon H, Cotten J (1993) High-Mg andesites from the southern termination of the New Hebrides island arc (SW Pacific). J Volcanol Geotherm Res 57:193–217

Münker C, Weyer S, Scherer E, Mezger K (2001) Separation of high field strength elements (Nb, Ta, Zr, Hf) and Lu from rock samples for MC-ICPMS measurements. Geochem Geophys Geosyst 2:2001GC000183

Peacock SM, Rushmer T, Thompson AB (1994) Partial melting of subducting oceanic crust. Earth Planet Sci Lett 121:227–244

Pearce JA, Kempton PD, Nowell GM, Noble SR (1999) Hf–Nd element and isotope perspective on the nature and provenance of mantle and subduction components in Western Pacific arc-basin systems. J Petrol 40:1579–1611

Peate DW, Pearce JA, Hawkesworth CJ, Colley H, Edwards CMH, Hirose K (1997) Geochemical variations in Vanuatu arc lavas: the role of subducted material and a variable mantle wedge composition. J Petrol 38:1331–1358

Perfit MR, Langmuir CH, Baekisapa M, Chappell BW, Johnson RW, Staudigel H, Taylor SR (1987) Geochemistry and petrology of volcanic rocks from the Woodlark basin: addressing questions of ridge subduction. Circum-Pac Counc Energy Miner Res 7:113–154

Petersen J (1891) Der Boninit von Peel Island. Jahrb Hambg Wiss Anst 8:341–349

Petterson MG, Babbs T, Neal CR, Mahoney JJ, Saunders AD, Duncan RA, Tolia D, Magu R, Qopoto C, Mahoa H, Natogga D (1999) Geological-tectonic framework of Solomon Islands, SW Pacific: crustal accretion and growth within an intra-oceanic setting. Tectonophysics 301:35–60

Rapp RP, Watson EB (1995) Dehydration melting of metabasalt at 8–32 kbar: implications for continental growth and crust–mantle recycling. J Petrol 35:891–931

Ringwood AE (1974) The petrological evolution of island arc systems. J Geol Soc Lond 130:183–204

Rohrbach A, Schuth S, Ballhaus C, Münker C, Matveev S, Qopoto C (2005) Petrological constraints on the origin of arc picrites, New Georgia Group, Solomon Islands. Contrib Mineral Petrol 149:685–698

Sajona FG (1995) Fusion de la croute océanique en contexte de subduction collision: géochimie, geochronology et pétrologie du magmatisme plioquaternaire de Mindano (Philippines). Unpublished thesis, Brest University, 223 pp

Schuth S, Rohrbach A, Münker C, Ballhaus C (2004) Geochemical constraints on the petrogenesis of arc picrites and basalts, New Georgia Group, Solomon Islands. Contrib Mineral Petrol 148:288–304

Sen C, Dunn T (1994) Dehydration melting of a basaltic composition amphibolite at 1.5 and 2.0 GPa – Implications for the origin of adakites. Contrib Mineral Petrol 117(4):394–409

Sobolev AV, Hofmann AW, Sobolev SV, Nikogosian TK (2005) An olivine-free mantle source of Hawaiian shield basalts. Nature 434:590–597

Stern CR, Kilian R (1996) Role of subducted slab, mantle wedge and continental crust in the generation of adakites from the Andean Austral Volcanic Zone. Contrib Mineral Petrol 123:263–281

Sun S-S, Nesbitt RW (1978) Geochemical regularities and genetic significance of ophiolitic basalts. Geology 6:68–93

Tatsumi Y (1982) Origin of high-magnesian andesites in the Setouchi volcanic belt, southwest Japan, II. Melting phase relations at high pressures. Earth Planet Sci Lett 60:305–317

Tejada MLG, Mahoney JJ, Neal CR, Duncan RA, Petterson MG (2002) Basement geochemistry and geochronology of Central Malaita, Solomon Islands, with implications for the origin and evolution of the Ontong Java Plateau. J Petrol 43:449–484

Todt W, Cliff RA, Hanser A, Hofman AW (1996) Evaluation of a ^{202}Pb–^{205}Pb double spike for high-precision lead isotope analysis. In: Earth processes: reading the isotope code. Geophysical Monograph 95, pp 429–437

Walker DA, Cameron WE (1983) Boninite primary magmas: evidence from Cape Vogel Peninsula, PNG. Contrib Mineral Petrol 83:150–158

Woodhead JD, Eggins SM, Johnson RW (1998) Magma genesis in the New Britain island arc: further insights into melting and mass transfer processes. J Petrol 39:1641–1668

Woodhead JD, Hergt JM, Davidson JP, Eggins SM (2001) Hafnium isotope evidence for 'conservative' element mobility during subduction zone processes. Earth Planet Sci Lett 192:331–346

Workman RK, Hart SR (2004) Major and trace element compositions of the depleted MORB mantle. Earth Planet Sci Lett 231:53–72

Yan CY, Kroenke LW (1993) A plate tectonic reconstruction of the Southwest Pacific, 0–100 Ma. In: Proceedings of ocean drilling project, Scientific results, pp 697–709

Yogodzinski GM (1995) Magnesian andesite in the western Aleutian Komandorsky region: implications for slab melting and processes in the mantle wedge. GSA Bull 7:505–519

Yogodzinski GM, Lees JM, Churikova TG, Dorendorf F, Wörner G, Volynets ON (2001) Geochemical evidence for the melting of subducting oceanic lithosphere at plate edges. Nature 9:500–504

Yoneshima S, Mochizuki K, Araki E, Hino R, Shinohara M, Suyehiro K (2005) Subduction of the Woodlark Basin at the New Britain Trench, Solomon Islands region. Tectonophysics 397:225–239